In-vivo Dopamine Sensing PEDOT:CNF Neural Probe Design and Simulation

Stefanus Wirdatmadja, Harshithaa Ganesan,
Lauri Sydänheimo, Leena Ukkonen
Tampere University
Tampere, Finland
{firstname.lastname}@tuni.fi

Merja Voutilainen
University of Helsinki
Helsinki, Finland
merja.h.voutilainen@helsinki.fi

***Abstract*—The electrochemical analysis is one of the most popular implementations of a dopamine-sensing brain implant. Its performance depends significantly on the interaction between the dopamine molecule and the working electrode. Carbon nanofiber is an allotrope of carbon nanotube and is effective in increasing the contact surface with dopamine molecules. Considering its simple fabrication protocols using photolithography, physical vapor deposition, and electrochemical deposition, this material is suitable for in-vivo implementation. COMSOL simulation confirms that carbon nanofiber implementation increases the redox current while maintaining its linearity to the user-controlled dopamine concentration.**

I. Introduction

In the field of neuroscience, brain implants play an important role in both chemical and electrophysiological recordings of brain activity. Intra- and inter-neuronal communication comprise the transmission of both chemical and electrical signals. Therefore, different signal detection techniques are used. For instantaneous electrophysiological signals (spikes) detection can be accommodated by electroencephalogram (EEG) and electrocorticography (ECoG). Since ECoG is implemented invasively, it overcomes EEG in terms of spatial resolution. The neuronal spikes have an amplitude of hundreds μV to a few mV [1]-[3]. Unlike brain electrical signal detection which can be done both non-invasively and invasively, neuronal chemical signals (neurotransmitters) should be done invasively. The invasiveness of the neurotransmitter sensor facilitates real-time monitoring and ensures data precision. Furthermore, direct contact with the brain tissue helps the device to target a certain area where the data should be gathered. For example, depending on the neuronal pathway (reward or motoric functions), dopamine can be detected in the ventral tegmental area (VTA) or red nucleus. Furthermore, the concentration range in those regions is different (4.8±1.5 nM in the VTA and 0.5±1.5 nM in the red nucleus) [4]. Thus, in-vivo sensor design for the neurotransmitter should consider these factors as it is the front-end element of the implant determining the quality of the raw data.

Dopamine has a critical role in many systems in central nervous systems such as modulating motor movement, cognitive functions, and reward as part of basal ganglia circuitry. These molecules can be analyzed electrochemically using voltammetry or amperometry techniques by exploiting their properties. Using these techniques, dopamine molecules are oxidized into dopamine-o-quinone at a voltage of 600 mV and the linearity of the oxidized current can be achieved for further analysis [5].

Various shapes and materials of sensing electrodes have been designed to accommodate the desired sensing location, sensitivity, and selectivity. Electrochemical working electrodes for implants can be an array consisting of microstructures for multi-point recording or a single-unit entity to target a small sensing area. Several studies have employed electrode arrays for dopamine monitoring applications. A working electrode array is used for dopamine release measurement from multiple points in the brain (the striatum, substantia nigra pars compacta (SNc), and VTA) to study behavioral performance and reward-related stimuli [6]. Other research groups implement microelectrode arrays (MEA) to facilitate a dopamine concentration measurement at different brain locations for simultaneous dopamine detection and electrical signals [7]-[9]. This structure accommodates various purposes such as concentration mapping and multiple detection methods. Unlike electrode arrays, a single-entity unit electrode usually focuses on a certain brain region and the electrode shape possesses a needle-like structure to improve precision in sensor implantation in the brain tissue. For Parkinson's disease (PD), dopamine concentration drops significantly in the dorsal striatum and corresponds to symptoms of motoric disorders such as tremors. Therefore, dopamine concentration measurement is focused on this region and the progression of this disease can be monitored [10], [11].

When electrochemical sensing is employed, carbon-based electrodes are considered a gold standard for in-vivo neurochemical detection analysis. These materials exhibit excellent properties such as biocompatibility, sensitivity, and adsorbability for electroactive substances [12]. Glassy carbon, carbon nanofiber, and graphene are some examples of carbon-based materials that have been used and studied, especially for dopamine detection [13]-[15]. Those materials can further be modified, manipulated, and functionalized to enhance their selectivity and adsorbability to dopamine.

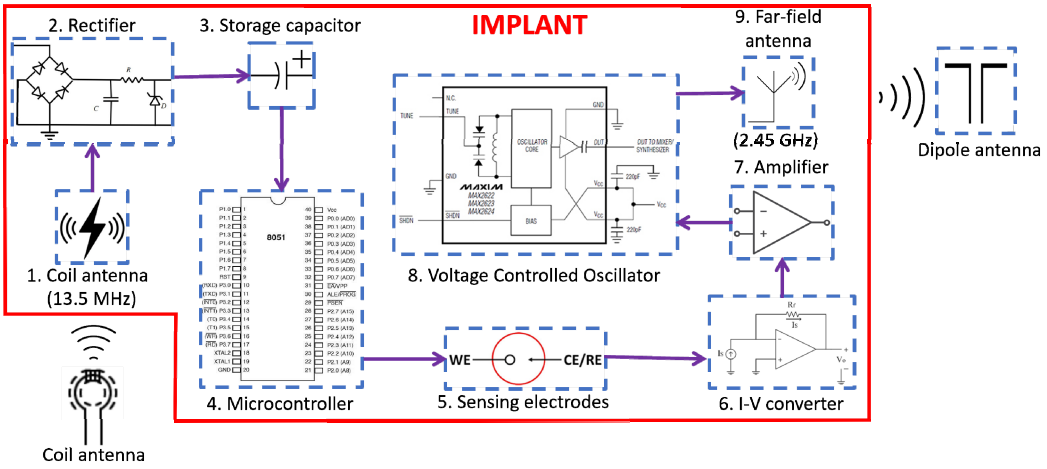

Fig 1. Implant components

In this publication, dopamine dopamine-sensing neural probe design is proposed with the carbon nanofiber (PEDOT:CNF) material as a working electrode, iridium oxide (IrOx) as a reference electrode, and platinum (Pt) as a counter electrode. The electrode adopts needle-like structure to measure dopamine concentration in the dorsal striatum region. The significance of electrode design employing carbon nanofibers (CNF) is simulated with COMSOL Multiphysics.

II. Implant Circuitry

The proposed sensor can support various brain implant implementations including the wireless sensing device. One wireless implementation option is to employ two antennas for power and data transmission depicted in Fig. 1. The coil antenna will receive the radio frequency (RF) power from the external coil antenna. The received power signal will be rectified and stored in the storage capacitor. This energy will be used to power the microcontroller for applying the cyclic voltammetry (CV) waveform to the working electrode (WE). After the dopamine undergoes the redox reaction, the oxidation current will be converted to an electrical voltage by an I-V converter. The voltage will then be amplified before being fed to the voltage-controlled oscillator (VCO). The raw data will be transmitted by the implant far-field antenna to the off-body dipole antenna for further data analysis [16]. In this publication, sensing electrodes, shown in Fig. 1 component 5, are further elaborated.

III. Electrode Materials

Carbon nanofibers (CNFs) are the emerging electrode nanomaterial for in-vivo electrochemical analysis due to their large surface area, non-toxicity, and electrochemical inertness. In electrochemistry, a larger surface area is desirable due to the easier electron transfer during the reduction and oxidation (redox) reaction, and the material's inertness is required to prevent reaction interference. Additionally, since CNF has a honeycomb lattice structure, the non-covalent interaction between the DA molecule's benzene ring contributes to the adsorption between them [17], [18]. These interactions are π-π, NH···π, and CH···π bonds. Finally, to accommodate electrochemical analysis, CNF electrodes have been designed in various shapes, such as cylinder and microelectrode array (MEA) [19], [20].

One of the most common reference electrode materials in electrochemistry is Ag/AgCl. However, this material suffers from degradation which causes inaccurate applied voltage to the working electrode. Moreover, the chronic implantation of Ag/AgCl electrodes leads to cell death and gliosis of the surrounding tissue [21], [22]. As a reference electrode, iridium oxide (IrOx) is categorized as polarized and pH-sensitive; nonetheless, it is a promising candidate for in vivo application due to its biocompatibility and long-term stability which is an excellent alternative to Ag/AgCl [23].

Platinum is used as the counter electrode of the proposed sensor design due to its high conductivity, chemically stable, and corrosion resistance. In electrochemical analysis, this electrode is used to complete and close the current circuit. When an oxidation reaction occurs at the working electrode, a corresponding reduction reaction occurs at the counter electrode. This results in no current flowing between the working and reference electrode and the working electrode potential change can be monitored accurately. Additionally, platinum has great mechanical properties in terms of ductility, low brittleness, and durability [24].

From those materials (CNFs, IrOx, and Pt), the proposed three-electrode configuration sensor is designed to target the substantia nigra, which is mostly populated by dopaminergic neurons (Fig. 2).

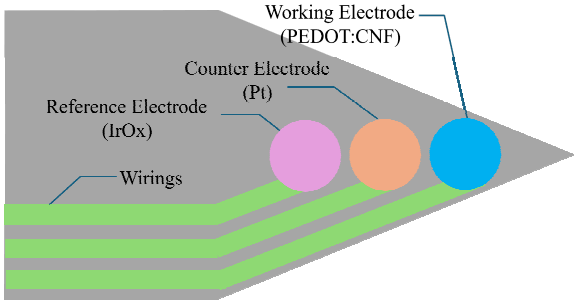

Fig. 2. Three-electrode structure

IV. Neural Probe Design

The neural probe, with dimensions of 50 mm by 2 mm, is designed to seamlessly integrate with the brain's complex structures for dopamine detection (Fig. 3). The needle-like shape is chosen to target limited area of substantia nigra. This electrochemical sensor includes circular electrodes for the working (WE), counter (CE), and reference (RE) electrodes, each with a 20 µm diameter and a center-to-center spacing of 0.5 mm, which can be adjusted as required for precise positioning. The square contact pads measure 1 mm on each side, providing ample surface area for robust connectivity. The sensor utilizes a silicon substrate to ensure optimal biocompatibility and mechanical stability. Platinum is employed for the contact pads and wiring to offer superior electrical performance and durability. The working electrode is innovatively crafted with carbon nanofiber (PEDOT:CNF) decorated over a gold electrode, enhancing its sensitivity and selectivity towards dopamine molecules. Iridium oxide (IrOx) forms the reference electrode, chosen for its excellent stability and reliable reference potential. Platinum is also used for the counter electrode, ensuring consistent performance and effective counterbalancing of the electrical current during sensing.

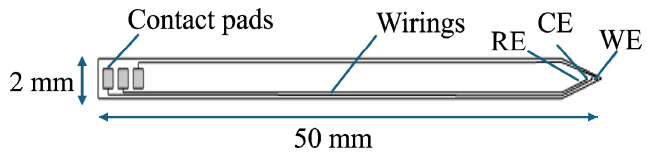

Fig. 3. Neural probe structure

V. Fabrication Protocol

To realize three different materials for the electrodes elaborated in Sec. III and IV, several common fabrication methods should be employed such as photolithography and physical vapor deposition (PVD) [20], [25]. The illustration of the fabrication protocol for the proposed sensor is depicted in Fig. 4 and the steps are elaborated as follows:

1) Silicon substrate wafer is precleaned by MW-oxygen plasma.
2) A negative photoresist layer is spin-coated and photopatterned for the working electrode.
3) Gold (Au) physical vapor deposition (PVD) metallization.
4) Lift off at room temperature by acetone overnight, leaving the Au layer as the working electrode.
5) A negative photoresist layer is spin-coated and photopatterned for the reference and counter electrodes.
6) Platinum (Pt) physical vapor deposition (PVD) metallization for both counter and reference electrodes.
7) Lift off at room temperature in acetone overnight.
8) Wafer cleaning by piranha solution and MW-oxygen plasma.
9) SU-8 spin-coating.
10) Photopatterning of SU-8 passivation layer for the insulation.
11) Pouring deposition solution (PEDOT:CNF) for electrochemical deposition process.
12) Applying 3.14 nA current until deposition charge reaches 1200 nC.
13) PEDOT:CNF is formed on top of Au.
14) DC sputter deposition of IrOx in an oxygen plasma.

VI. COMSOL Simulation

A. Simulation Model

For the 2D modelling, the brain tissue is modelled as a square with size 50 x 50 µm with the material polyimide with Poisson's ratio 0.33 (Fig. 5) [26]. At the bottom surface, the WE (gold) base of diameter 20 µm is placed with a 10-CNF arrangement each having a length of 5 µm and an average fiber radius of 0.2 µm. The other remaining boundary is the silicon substrate acting as an insulating layer. We applied a user-controlled mesh with triangular meshing over the brain domain with the predefined finer elements and extremely finer elements in the CNF region (Fig. 6).

B. Electrochemical analysis

The electrochemical analysis using COMSOL Multiphysics for dopamine detection in the brain involves specific parameters and equations designed for precision and accuracy. The temperature (T) is controlled at 298.15 K, providing a stable environment for electrochemical reactions. The diffusion coefficient of dopamine (D_{dop}) is set at 8.2×10^{-11} m^2/s, reflecting the rate at which dopamine molecules diffuse through the medium. The reference exchange current density (i^0_{ref}) is determined as 1000 mol/(m^2/s)× F, where F represents the Faraday constant (96485.7 A·s/mol), indicating the standard rate of electron exchange at the electrode surface.

Initial concentrations are crucial, with dopamine (C^0_{dop} at 1 mol/m^3) and dopamine-o-quinone (C^0_{dopox} at 0.001 mol/m^3), representing the reactant and product species which is 1000 times smaller than the reactant. The scan rate (υ) is maintained at 1 V/s, a moderate rate that allows for adequate reaction observation. The reaction rate constant (k^0) is set at 1000 M/s, signifying the intrinsic speed of the electron transfer process. A double-layer capacitance (C_{dl} at 0.01F/m^2) is used to account for the capacitive effects at the electrode interface. The double-layer capacitance is a measure of the charge storage at the electrode interface due to the separation of charges in the electrode and the electrolyte. It plays a significant role in the capacitive charging current, which must be differentiated from the faradaic current in the electrochemical measurements.

For the cyclic voltammetry study, the Vertex potentials are determined at $E_{vertex1}$ = -0.5 V and $E_{vertex2}$ = 0.5 V. Sweeping between these potentials allows the system to explore both the oxidation and reduction processes of dopamine, providing an overview of the electrochemical behavior. The outer bound diffusion layer thickness (L) is calculated using the formula:

$$L = 6\sqrt{\frac{2|E_{vertex1} - E_{vertex2}|D_{dop}}{v}} \quad (1)$$

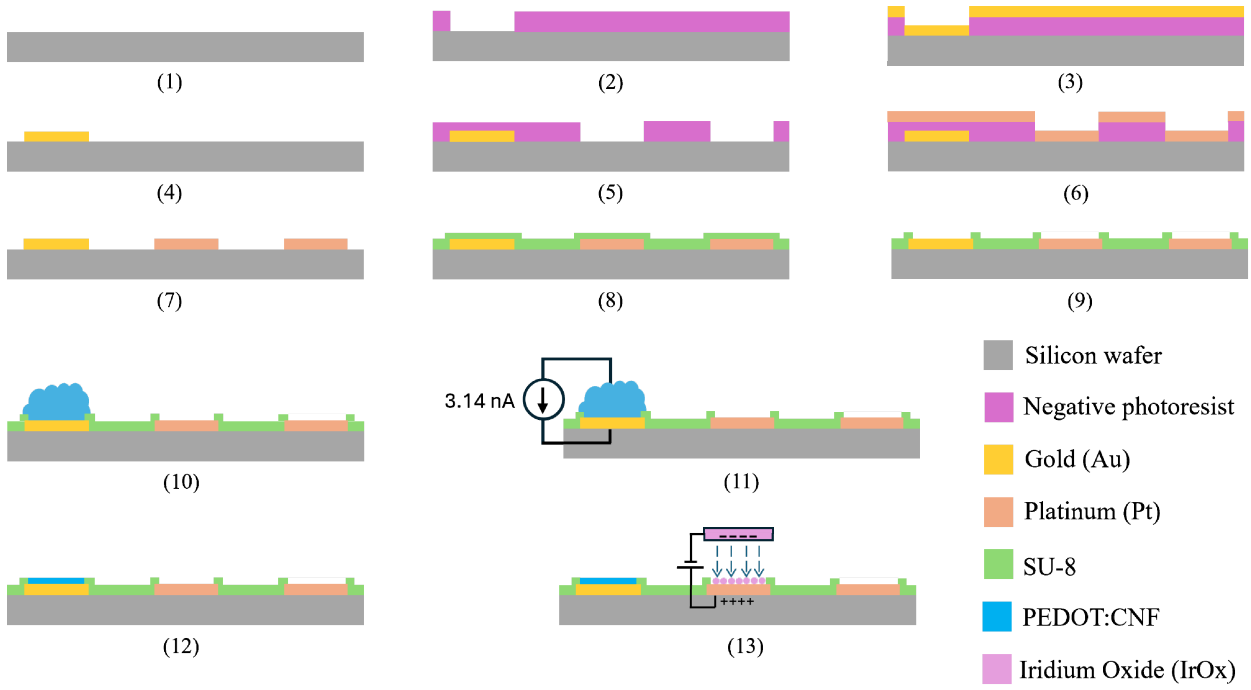

Fig. 4. Illustration of fabrication protocol

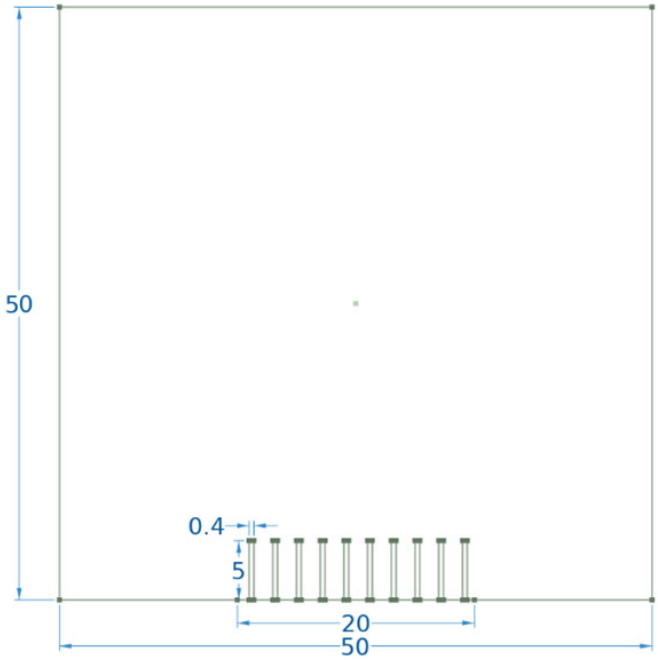

Fig. 5. COMSOL 2D simulation model

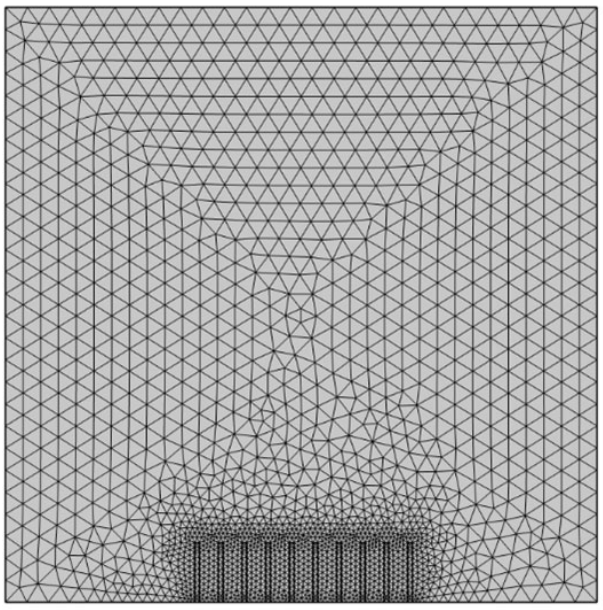

Fig. 6. COMSOL mesh model with 10 CNFs with 5-nm fiber thickness in a 50 x 50 brain matrix

which provides the characteristic length over which diffusion is significant. The initial product formation at the electrode surface (C_{B0}) is given by Eq. 2.

$$C_{B0} = \frac{C^0_{dop}}{1 + e^{-\frac{E_{vertex1}F}{RT}}} \quad (2)$$

where R is the gas constant (8.314 J/mol·K), representing the equilibrium concentration of the oxidized species at the electrode surface. The initial values for dopamine concentration (C_{dop}) and dopamine-o-quinone concentration (C_{dopox}) are crucial for setting up the boundary conditions for the system. These initial values are given by Eq. 3 and 4.

$$C_{dop} = abs(C^0_{dop} - C_{B0} \times (1 - \frac{x}{L})) \quad (3)$$

$$C_{dopox} = abs(C_{B0} \times -(1 - \frac{x}{L})) + C^0_{dopox} \quad (4)$$

In the electrode phase potential analysis, cyclic voltammetry (CV) is employed with a scan rate of 1 V/s over 10 cycles (Fig. 7), sweeping between -0.5 V and 0.5 V. This method captures the current response as a function of the applied voltage, providing detailed insights into the dopamine oxidation kinetics and mechanisms. The Nernst-Planck equation relates the electrode potential to the concentrations of oxidized and reduced forms of dopamine, characterizing the equilibrium at the electrode surface. The Butler-Volmer equation models the kinetics of electron transfer processes, incorporating factors such as overpotential and exchange current density. The electron transfer process involves two electrons per reaction, with a stoichiometric coefficient of 1 for dopamine and -1 for dopamine-o-quinone. A cyclic voltammetry-based study is carried out in COMSOL Multiphysics to analyze the importance of CNF and the concentration study of dopamine. This comprehensive electrochemical setup allows for a detailed understanding of neurotransmitter dynamics under physiological conditions, crucial for advancing neurochemical sensing technology.

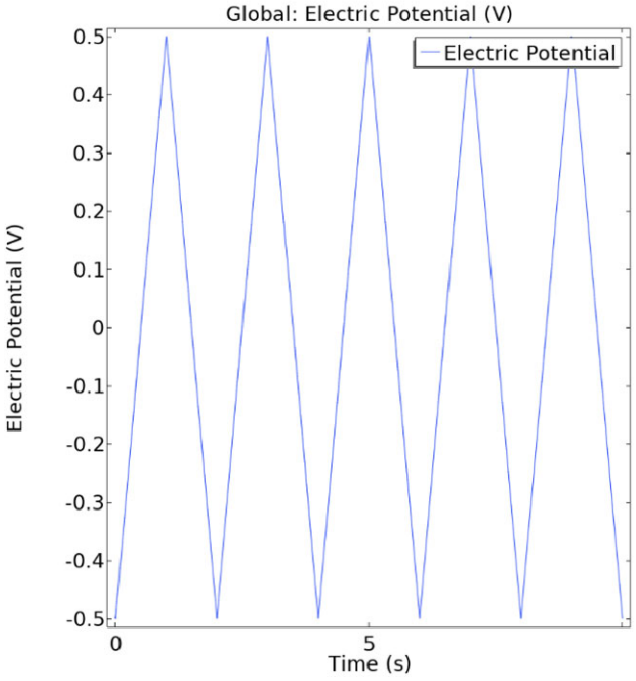

Fig. 7. Triangular waveform for cyclic voltammetry with a scan rate of 1 V/s (10 cycles)

VII. Results and Discussion

A. Importance of CNF

Table I and II reveal the complex relationship between the CNF thickness (T = 1, 2, 5, 10 µm), and different densities of carbon nanofibers (CNF = 0, 5, 10, 15, 20), and their impact on the total current (I_{tot}) and average current density (J_{avg}) in dopamine sensing applications.

Without CNF, the electrode shows lower total current values, which suggests limited electron transfer efficiency. As the CNF density increases, the total current improves significantly across all CNF thicknesses, indicating that CNFs enhance electron transfer at the electrode interface. This enhancement is particularly evident in thicker CNF (T = 5 µm and 10 µm), where higher CNF density leads to an increased total current. The increase in surface area provided by the CNFs enables more active sites for electron transfer, thereby increasing the total current. In the case of the electrode without CNFs (just gold), the smaller surface area reduces the available active sites for electron transfer, resulting in a lower total current. This aligns with the relationship described by Eq 5.

$$J_{avg} = \frac{I_{tot}}{A_{WE}} \quad (5)$$

where increasing surface area A_{WE} via CNFs allows for higher current to maintain a relatively consistent current density.

TABLE I. Total current for different CNF density (0, 5, 10, 15, and 20) with different thickness (1, 2, 5, and 10 µM)

Total current (A)	T=1 µm	T=2 µm	T=5 µm	T=10 µm
Without CNF	-1.34E-11	-	-	-
5 CNFs	-1.37E-11	-1.48E-11	-1.88E-11	-2.61E-11
10 CNFs	-1.41E-11	-1.57E-11	-2.05E-11	-2.89E-11
15 CNFs	-1.45E-11	-1.62E-11	-2.12E-11	-3.02E-11
20 CNFs	-1.48E-11	-1.67E-11	-2.23E-11	-3.20E-11

In terms of average current density, as the diffusion layer thickness increases, the current density decreases for all CNF densities, which is consistent with a reduced concentration gradient of dopamine near the electrode surface. The drop in current density is most pronounced at higher CNF densities and larger CNF thicknesses. However, this does not imply a reduction in overall performance, as the increased surface area due to CNFs allows for higher total current while maintaining current density. Therefore, the CNFs contribute both by enhancing the electrode's active surface area and by improving the overall electrochemical performance, making them critical for optimizing in vivo dopamine detection. Balancing CNF density with diffusion layer thickness is essential for ensuring both enhanced sensitivity and efficient current distribution in these sensors.

TABLE II. AVERAGE CURRENT DENSITY FOR DIFFERENT CNF DENSITY (0, 5, 10, 15, AND 20) WITH DIFFERENT FIBER THICKNESSES (1, 2, 5, AND 10 μM)

Average current density (A/m^2)	T=1 μm	T=2 μm	T=5 μm	T=10 μm
Without CNF	-0.66780	-	-	-
5 CNFs	-0.45588	-0.37098	-0.26828	-0.21780
10 CNFs	-0.35353	-0.26144	-0.17048	-0.13134
15 CNFs	-0.29065	-0.20226	-0.12498	-0.09447
20 CNFs	-0.24733	-0.16740	-0.10147	-0.07628

B. *Concentration Study*

The voltammogram demonstrates the electrochemical behavior of dopamine under varying electric potentials (Fig. 8). The symmetrical, duck-shaped curve suggests a reversible redox reaction, characteristic of dopamine oxidation and reduction. The peak currents correspond to the oxidation and reduction of dopamine, and the multiple overlaid curves indicate that this study may involve different conditions, such as varying dopamine concentrations or surface modifications (e.g., CNF integration). As electric potential moves in the positive direction, dopamine is oxidized, leading to an anodic peak in current. Conversely, in the negative direction, dopamine is reduced, resulting in a cathodic peak. The current magnitude increases with the scan rate, surface area, or concentration of dopamine, implying efficient electron transfer during the redox process.

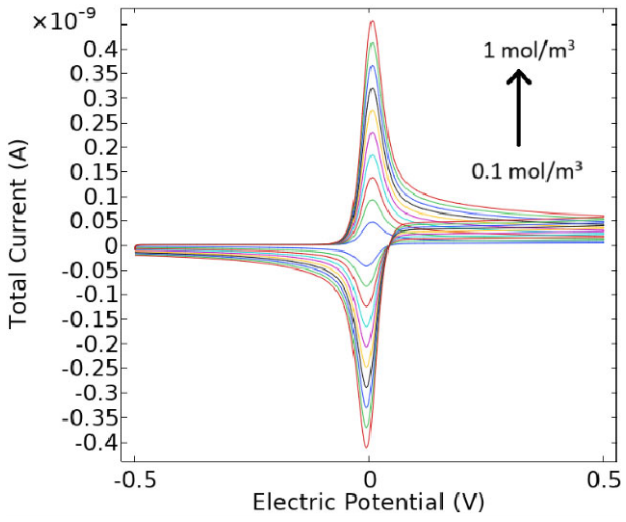

Fig. 8. Voltammograms for dopamine concentration from 0.1 mol/m^3 to 1 mol/m^3 at 1 V/s

The plot in Fig. 9 indicates a linear relationship between the current density and the initial reactant concentration (dopamine) in the bulk solution. As the concentration increases from 0 to 1 mol/m^3, the current density (A/m^2) decreases linearly. This trend suggests that higher dopamine concentrations lead to lower current densities at the electrode surface. This inverse relationship could be explained by the diffusion-limited behavior of the electrochemical process. At higher concentrations, dopamine molecules near the electrode are consumed faster than they can be replenished by diffusion from the bulk, leading to a decrease in current density. The concentration profile for the dopamine-o-quinone (the oxidized form of dopamine) is depicted in Fig. 10.

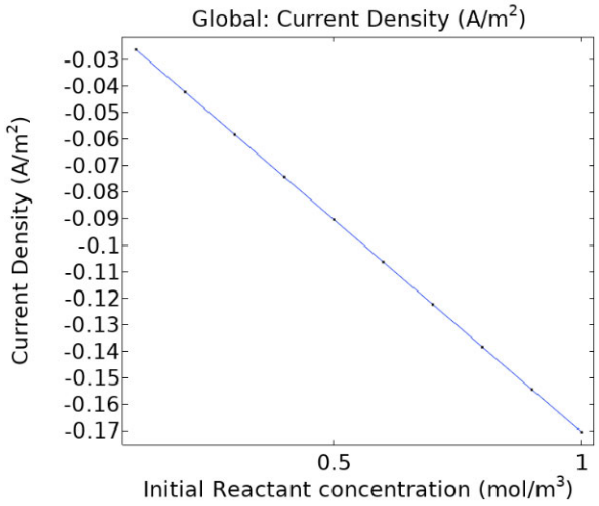

Fig. 9. The linear relationship between average current density and dopamine concentration

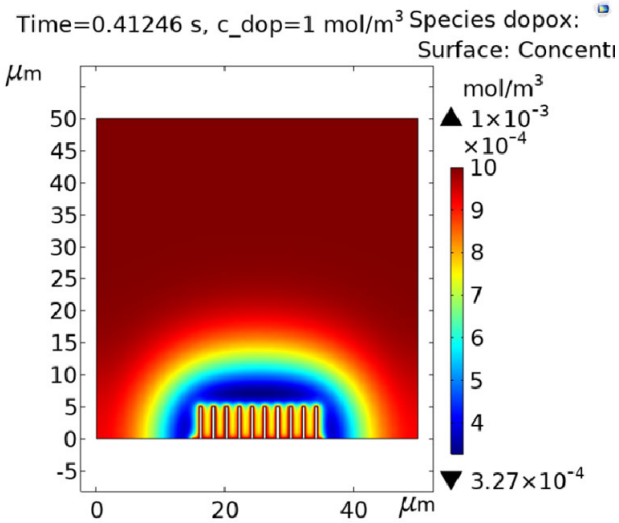

Fig. 10. Concentration profile of the dopamine-o-quinone

These findings underline the importance of optimizing dopamine concentration, scan rate, and electrode surface area to achieve sensitive and accurate dopamine detection. CNF contributes significantly to increasing the electrode surface area.

REFERENCES

[1] C. Gold, D. A. Henze, C. Koch, and G. Buzsaki, "On the origin of the extracellular action potential waveform: a modeling study," *Journal of Neurophysiology*, vol. 95, no. 5, pp. 3113–3128, 2006.

[2] J. E. Chung, H. R. Joo, J. L. Fan, D. F. Liu, A. H. Barnett, S. Chen, C. Geaghan-Breiner, M. P. Karlsson, M. Karlsson, K. Y. Lee et al., "High-density, long-lasting, and multi-region electrophysiological recordings using polymer electrode arrays," *Neuron*, vol. 101, no. 1, pp. 21–31, 2019.

[3] N. A. Steinmetz, C. Aydin, A. Lebedeva, M. Okun, M. Pachitariu, M. Bauza, M. Beau, J. Bhagat, C. Böhm, M. Broux et al., "Neuropixels 2.0: A miniaturized high-density probe for stable, long-term brain recordings," *Science*, vol. 372, no. 6539, p. eabf4588, 2021.

[4] T. R. Slaney, O. S. Mabrouk, K. A. Porter-Stransky, B. J. Aragona, and R. T. Kennedy, "Chemical gradients within brain extracellular space measured using low flow push–pull perfusion sampling in vivo," *ACS Chemical Neuroscience*, vol. 4, no. 2, pp. 321–329, 2013.

[5] S. Wirdatmadja, W. Ventilä, J. Vesanen, T. Björninen, R. Lahtinen, L. Sydänheimo, M. Voutilainen, and L. Ukkonen, "Wireless carbon-based electrochemical dopamine sensor brain implant," in *2023 IEEE 13th International Conference on RFID Technology and Applications (RFID-TA)*. IEEE, 2023, pp. 115–118.

[6] H. N. Schwerdt, H. Shimazu, K.-i. Amemori, S. Amemori, P. L. Tierney, D. J. Gibson, S. Hong, T. Yoshida, R. Langer, M. J. Cima et al., "Long-term dopamine neurochemical monitoring in primates," *Proceedings of the National Academy of Sciences*, vol. 114, no. 50, pp. 13 260–13 265, 2017.

[7] E. Castagnola, N. W. Vahidi, S. Nimbalkar, S. Rudraraju, M. Thielk, E. Zucchini, C. Cea, S. Carli, T. Q. Gentner, D. Ricci et al., "In vivo dopamine detection and single unit recordings using intracortical glassy carbon microelectrode arrays," *MRS Advances*, vol. 3, no. 29, pp. 1629–1634, 2018.

[8] G. Xiao, Y. Song, Y. Zhang, Y. Xing, H. Zhao, J. Xie, S. Xu, F. Gao, M. Wang, G. Xing et al., "Microelectrode arrays modified with nanocomposites for monitoring dopamine and spike firings under deep brain stimulation in rat models of Parkinson's disease," *ACS Sensors*, vol. 4, no. 8, pp. 1992–2000, 2019.

[9] D.-S. Kim, E.-S. Kang, S. Baek, S.-S. Choo, Y.-H. Chung, D. Lee, J. Min, and T.-H. Kim, "Electrochemical detection of dopamine using periodic cylindrical gold nanoelectrode arrays," *Scientific Reports*, vol. 8, no. 1, p. 14049, 2018.

[10] B. Wang, X. Wen, Y. Cao, S. Huang, H. A. Lam, P.-S. Chung, H. G. Monbouquette, P.-Y. Chiou, N. T. Maidment et al., "An implantable multifunctional neural microprobe for simultaneous multi-analyte sensing and chemical delivery," *Lab on a Chip*, vol. 20, no. 8, pp. 1390–1397, 2020.

[11] Z. Shao, H. Zhao, K. E. Dunham, Q. Cao, N. V. Lavrik, and B. J. Venton, "3D-printed carbon nanoneedle electrodes for dopamine detection in drosophila," *Angewandte Chemie*, p. e202405634, 2024.

[12] B. J. Venton and Q. Cao, "Fundamentals of fast-scan cyclic voltammetry for dopamine detection," *Analyst*, vol. 145, no. 4, pp. 1158–1168, 2020.

[13] C. B. A. Hassine, H. Kahri, and H. Barhoumi, "Enhancing dopamine detection using glassy carbon electrode modified with graphene oxide, nickel and gold nanoparticles," *Journal of The Electrochemical Society*, vol. 167, no. 2, p. 027516, 2020.

[14] A. Kousar, I. Pande, L. F. Pascual, E. Peltola, J. Sainio, and T. Laurila, "Modulating the geometry of the carbon nanofiber electrodes provides control over dopamine sensor performance," *Analytical Chemistry,* vol. 95, no. 5, pp. 2983–2991, 2023.

[15] M. Kujawska, S. K. Bhardwaj, Y. K. Mishra, and A. Kaushik, "Using graphene-based biosensors to detect dopamine for efficient Parkinson's disease diagnostics," *Biosensors*, vol. 11, no. 11, p. 433, 2021.

[16] M. H. Behfar, L. Sydänheimo, S. Roy, and L. Ukkonen, "Dual-port planar antenna for implantable inductively coupled sensors," *IEEE Transactions on Antennas and Propagation,* vol. 65, no. 11, pp. 5732–5739, 2017.

[17] A. C. R. Fernández and N. J. Castellani, "Dipole moment effects in dopamine/n-doped-graphene systems," *Surface Science*, vol. 693, p. 121546, 2020.

[18] A. C. R. Fernández and N. J. Castellani, "Noncovalent interactions between dopamine and regular and defective graphene," *ChemPhysChem*, vol. 18, no. 15, pp. 2065–2080, 2017.

[19] J. E. Koehne, M. Marsh, A. Boakye, B. Douglas, I. Y. Kim, S.-Y. Chang, D.-P. Jang, K. E. Bennet, C. Kimble, R. Andrews et al., "Carbon nanofiber electrode array for electrochemical detection of dopamine using fast scan cyclic voltammetry," *Analyst*, vol. 136, no. 9, pp. 1802–1805, 2011.

[20] V. Saunier, E. Flahaut, M.-C. Blatché, C. Bergaud, and A. Maziz, "Microelectrodes from pedot-carbon nanofiber composite for high performance neural recording, stimulation and neurochemical sensing," *MethodsX*, vol. 7, p. 101106, 2020.

[21] E. M. Robbins, E. Castagnola, and X. T. Cui, "Accurate and stable chronic in vivo voltammetry enabled by a replaceable subcutaneous reference electrode," *Iscience*, vol. 25, no. 8, 2022.

[22] W. F. Jackson and B. R. Duling, "Toxic effects of silver-silver chloride electrodes on vascular smooth muscle." *Circulation Research*, vol. 53, no. 1, pp. 105–108, 1983.

[23] B. T. Seaton and M. L. Heien, "Biocompatible reference electrodes to enhance chronic electrochemical signal fidelity in vivo," *Analytical and Bioanalytical Chemistry*, vol. 413, no. 27, pp. 6689–6701, 2021.

[24] G. Jerkiewicz, "Applicability of platinum as a counter-electrode material in electrocatalysis research," *ACS Catalysis*, vol. 12, no. 4, pp. 2661–2670, 2022.

[25] R. K. Franklin, S. Joo, S. Negi, F. Solzbacher, and R. B. Brown, "A comparison of fabrication methods for iridium oxide reference electrodes," in SENSORS, 2009 IEEE. IEEE, 2009, pp. 1086–1089.

[26] S. Han, M. Polanco, H. Yoon, and S. Bawab, "Simulation of neurotransmitter sensing by cyclic voltammetry under mechanical motion of a neural electrode," *Brain*, vol. 13, no. 15000, pp. 0–45, 2017.